Electronic Supplementary Material (ESI) for Journal of Materials Chemistry A

Above 1% efficiency of a ferroelectric solar cell based on the $Pb(Zr, Ti)O_3$ film

Fengang Zheng,[a,b,]* Yu Xin,[a]* Wen Huang,[b,c] Jinxing Zhang,[d,e]Xiaofeng Wang,[a] Mingrong Shen,[a]

Wen Dong,[a] Liang Fang,[a] Yongbin Bai,[f] Xiaoqing Shen,[f] Jianhua Hao,[b]*

***Corresponding authors should be addressed:**

zhfg@suda.edu.cn; xylzf_1999@suda.edu.cn; jh.hao@polyu.edu.hk

Figure S1. Experimental details of a-Si/PZT/ITO/glass sample.

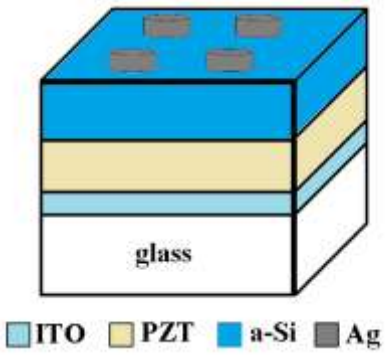

Figure S1 Structure sketch of Ag/a-Si/PZT/ITO/glass samples.

The ferroelectric $Pb(Zr_{0.2}Ti_{0.8})O_3$ (PZT) films were prepared by a sol-gel method on the ITO/glass substrates. The sol-gel experimental details can be seen in our previously published works.[1,2] The optimal thicknesses of a-Si (400 nm), PZT (330 nm), and ITO (120 nm) films were checked from the cross-sectional picture of a-Si/PZT/ITO/glass sample. For electrical and photocurrent measurements, about 80 nm thick Pt and Ag dots with a diameter of 0.2 mm were sputtered onto the PZT and a-Si/PZT films at room temperature, respectively, forming a typical Pt/PZT/ITO and Ag/a-Si/PZT/ITO capacitors, as shown in Figure S1. In the Ag/a-Si/PZT/ITO capacitors, Ag was used in order to form the ohmic contact between Ag electrode and a-Si film, which has been widely used in the amorphous silicon solar cells.[3]

Figure S2. XRD patterns and Raman spectra.

Figure S2a shows the XRD patterns of PZT/ITO/glass and a-Si/PZT/ITO/glass samples. XRD pattern of PZT/ITO/glass implies that PZT film is a polycrystalline system with a pure tetragonal perovskite phase. From the XRD pattern of a-Si/PZT/ITO/glass sample, no diffraction peak associated with crystalline silicon was

found except for some weak peaks from PZT film. In order to confirm the formation of an amorphous silicon film deposited on the PZT/ITO/glass substrate, we checked the Raman spectra of a-Si film, as shown in Figure S2b. The Raman spectra of a-Si film is composed of four Gaussian peaks: transverse optic (TO), longitudinal optic (LO), longitudinal acoustic (LA) and transverse acoustic (TA) modes, which are in accord with the other published work.[4] Compared with the standard Raman spectra of a-Si film,[4,5] the wavenumber of TO band and its line-width reflect a well short-range order of amorphous silicon network. However, the presence of LA mode and a high value in the integrated intensity of I_{LA}/I_{TO} ratio indicates the existence of quite a number of defects in the a-Si film.

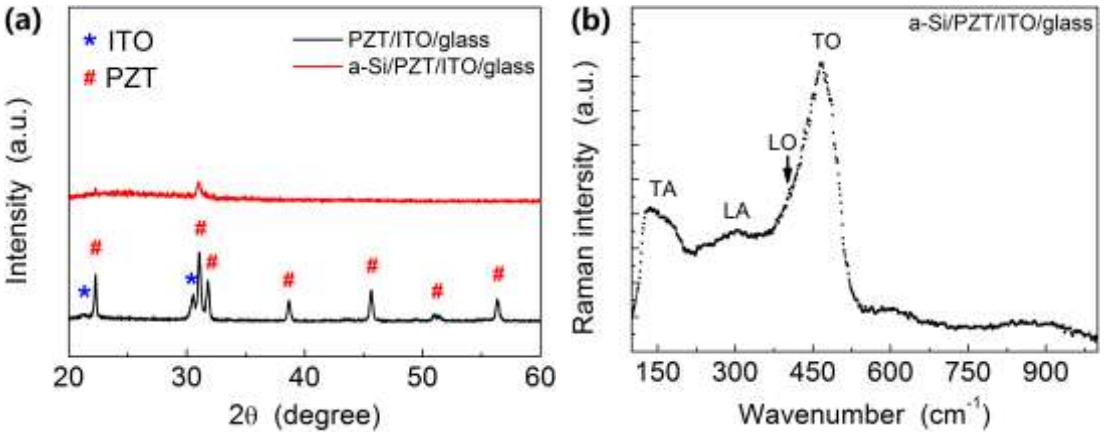

Figure S2. a. XRD patterns of PZT/ITO/glass and a-Si/PZT/ITO/glass samples. b. Raman spectra of a-Si film.

Figure S3. Hysteresis polarization loops of the samples

Figure S3 shows that PZT film has a typical hysteresis polarization loop and $2P_r$ of PZT film is about 40.7 μC/cm^2. However, the loop of PZT film shifts toward the positive branch (voltage offset), which is implied by the asymmetry between the

positive coercive field ($+E_c$, 164 kV/cm) and the negative coercive field ($-E_c$, 94 kV/cm). It is well-known that the asymmetry between $+E_c$ and $-E_c$ reflects a presence of the built-in filed in the ferroelectric film sandwiched by the top and bottom electrode.[6] Our previously published works[7,8] had confirmed that the built-in field was attributed to the difference between the Schottky barrier ($E_{bi\text{-}bottom}$) of the bottom electrode/film interface and the top one ($E_{bi\text{-}top}$). In the Pt/PZT/ITO/glass structure, $E_{bi\text{-}bottom}$ and $E_{bi\text{-}top}$ are back-to-back, and the difference between $E_{bi\text{-}bottom}$ and $E_{bi\text{-}top}$ is about 0.7 eV.[1] It is informed from Figure S3 that the introduction of a-Si film aggravates the asymmetry between $+E_c$ (188 kV/cm) and $-E_c$ (32 kV/cm), which reflects an existence of a larger built-in field in Ag/a-Si/PZT/ITO/glass sample. It is reasonable that this change of the built-in field could be attributed to the top a-Si/PZT interface because both the bottom PZT/ITO interface in the Ag/a-Si/PZT/ITO/glass sample and that in the Pt/PZT/ITO/glass sample are prepared under similar deposited condition.

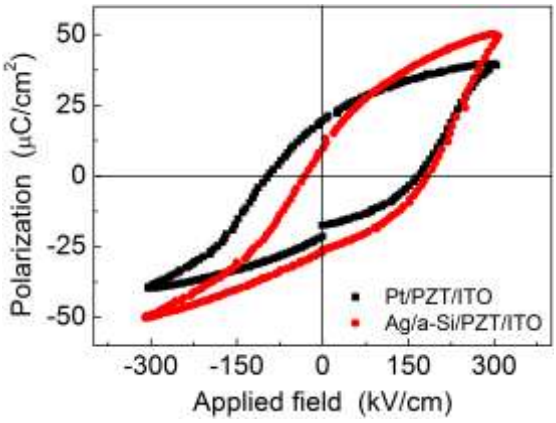

FigureS3. Hysteresis polarization loops of Pt/PZT/ITO/glass and Ag/a-Si/PZT/ITO/glass samples.

Note that PZT film in the Ag/a-Si/PZT/ITO/glass sample was kept unavoidably in vacuum at 300 ^{o}C for about 60 min during the deposition of a-Si film by sputtering,

which may result in an increase of the oxygen vacancy of PZT film, as a result, both remnant polarization and $E_{bi\text{-}bottom}$[9,10] decrease slightly. Both $2P_r$ (36.3μC/cm^2) and $2E_c$ (220 kV/cm) of Ag/a-Si/PZT/ITO/glass sample are slightly smaller than those of Pt/PZT/ITO/glass sample ($2P_r$: 40.7 μC/cm^2 and $2E_c$: 258 kV/cm, respectively), implying the increase of the oxygen vacancy of PZT film has little effect on the measured results, which could be almost neglected.

Figure S4. Transmissivity spectrum and band gaps of a-Si and PZT films

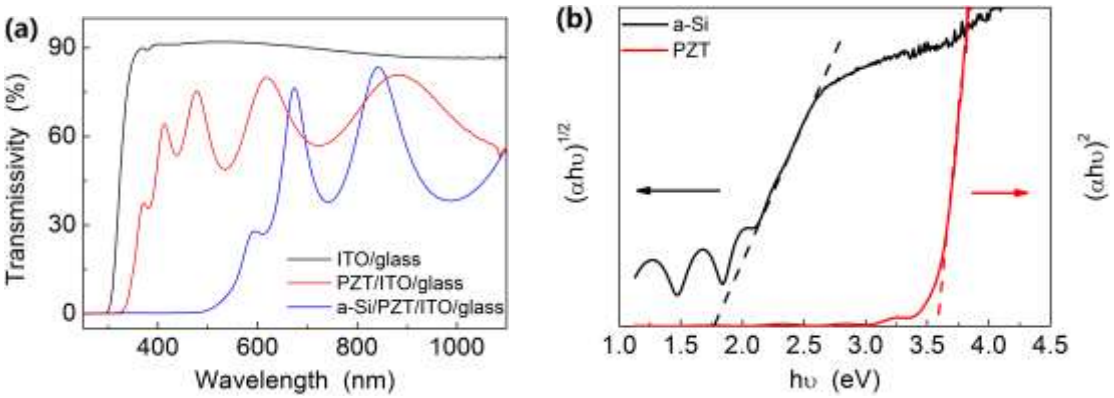

Figure S4. a. Transmissivity spectrum of PZT/ITO/glass and a-Si/PZT/ITO/glass samples. As a reference, the transmissivity and absorbance spectrum of ITO/glass substrate are also shown here. b. Band gaps of a-Si and PZT films calculated from the absorbance spectra of PZT/ITO/glass and a-Si/PZT/ITO/glass samples.

Figure S4a shows the transmissivity spectrum of PZT/ITO/glass and a-Si/PZT/ITO/glass samples. The absorption edge of PZT/ITO/glass is about 340 nm, corresponding to the band gap of PZT film. For the a-Si/PZT/ITO/glass samples, the absorption edge shifts to 500 nm. The optical band gap E_g can be determined from absorption coefficient α, calculated according to Tauc's relation using the following

equation:[11]

$$\alpha h\nu = A(h\nu - E_g)^m$$

where $h\nu$ is the photon energy, A is a constant, m is equal to 1/2 or 2 for direct or indirect gap materials, respectively. Because the PZT film is a direct band gap material,[1] the curve (red line) of the $(\alpha h\nu)^2$ versus $h\nu$ is linear near the absorption band regions, as shown in Figure S4b. However, the curve of the $(\alpha h\nu)^{1/2}$ versus $h\nu$ is widely used to define the band gap in the amorphous silicon (black line),[12] as shown in Figure S4b. The band gaps of a-Si and PZT layers are 1.8 and 3.6 eV, respectively, which are derived by extrapolating the linear part of the curves to the photo energy ($h\nu$) axis at α=0.

Figure S5. Transmissivity spectra of four filters named as K9, JB400, JB420, and ZWB2

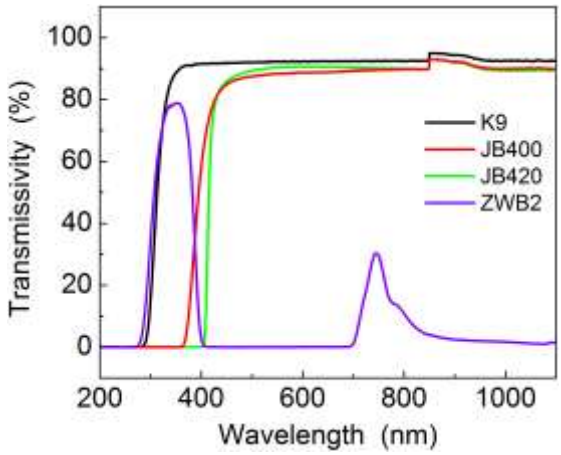

Figure S5. Transmissivity spectra of four filters named as K9 (black line), JB400 (red line), JB420 (green line), and ZWB2 (purple line), respectively.

Figure S5 shows the transmissivity spectra of four filters named as K9 (black line), JB400 (red line), JB420 (green line), and ZWB2 (purple line), respectively. The

absorption edges of K9, JB400, and JB420 filters are 290 nm, 370 nm, and 400 nm, respectively. ZWB2 is a band-pass filter. In the UV-visible waveband (200-700 nm), the short and long cutoff wavelengths of the ZWB2 filter are 280 nm and 400 nm, respectively. In the infrared band (700-1100 nm), ZWB2 filter has another passband (700-850 nm), which could be neglected here because the light (>700 nm) can not be absorbed by both PZT film and a-Si layer.

Figure S6. UPS spectra of a-Si film.

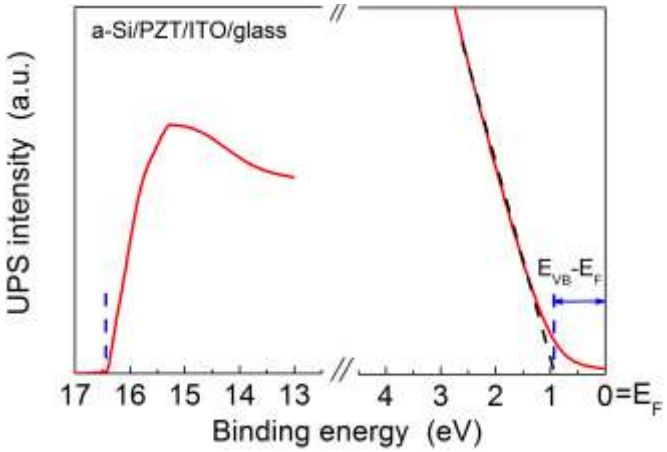

Figure S6. UPS cutoff spectra of a-Si film from the a-Si/PZT/ITO/glass sample. Left panel is the work function and right panel is the valence band region, respectively.

The energy levels of a-Si layer were determined by using an inelastic secondary electron cutoff of the ultraviolet photoelectron spectroscopy (UPS) energy distribution curve. This method[13,14] does not depend on any experimental parameters except for the photon energy of UV source (in our case He I discharge at hν = 21.21 eV). Figure S6 displays the typical UPS data of a-Si layer with a thickness of 400 nm. The work function ($\varphi = V_O - E_F$, V_O is the vacuum energy level and E_F is the Fermi level) of a-Si layer can be derived from the low kinetic energy cut-off in the secondary

emission features. The valence band (VB) maximum energy E_{VB} with respect to E_F is extrapolated by the linear portion of the low binding energy side of the proper VB peak to the energy axis,[15] as indicated in Figure S6. The measured φ of a-Si film is 21.21-16.43 = 4.78 eV. The energy difference between the E_F and E_{VB} for the a-Si film is about 0.93 eV as shown in Figure S6, indicating that the E_F of a-Si film is at the center of the band gap (1.8 eV, Figure S4)

Figure S7. Schematic energy diagram of Pt/PZT/ITO/glass sample.

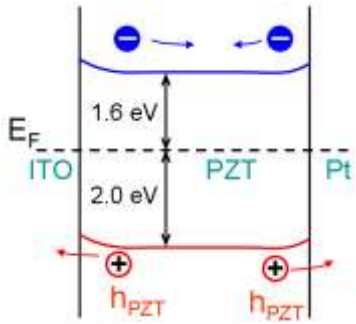

Figure S7. Schematic energy diagram of Pt/PZT/ITO/glass sample.

The conduct and valance band data can be seen in our previous work[1]. In the Pt/PZT/ITO/glass, the top Schottky barrier ($E_{bi\text{-}bottom}$) of Pt/PZT interface and the bottom one ($E_{bi\text{-}top}$) of PZT/ITO interface are back-to-back, as shown in Figure S7, and the $E_{bi\text{-}bottom}$ is higher 0.7 eV than the $E_{bi\text{-}top}$.[1] The UV light-induced holes are drifted to ITO electrodes and the electrons are expelled to Pt electrode. A part of the electrons arrived at the top Pt electrode are expelled back to the PZT film at the Pt/PZT interface because the direction of the $E_{bi\text{-}top}$ is opposite to that of the $E_{bi\text{-}bottom}$. When the PZT film is remnant polarization-up state, the depolarization field pointed from Pt to ITO electrode (not shown here), which is helpful for separating

light-induced electron-hole pairs.

Figure S8. Energy diagram of n-a-Si and p-a-Si films contacted with PZT film.

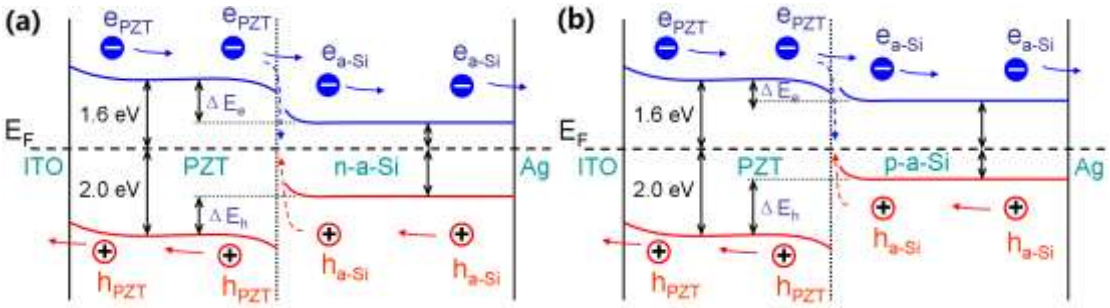

Figure S8. Energy diagram of Ag/n-a-Si/PZT/ITO/glass (a) and Ag/p-a-Si/PZT/ITO/glass samples (b).

An n-a-Si (P doped) and a p-a-Si (B doped) films were deposited on the PZT/ITO/glass substrates by sputtering, respectively, at the same condition as that of the a-Si film preparation. The target for the n-a-Si film is impurity phosphorus (P) doped n-type silicon monocrystal (P concentration of 1×10^{19} cm^{-3}), and that for the p-a-Si film is a boron (B) doped p-type silicon monocrystal (B concentration of 1×10^{19} cm^{-3}). The doping concentration of n-a-Si film is about 4.6×10^{17} cm^{-3}, which is slightly lower than that of p-a-Si film (about 7.4×10^{17} cm^{-3}). However, the dark conductivity of n-a-Si film is about 1.1×10^{-5} S/cm, which is higher than that of p-a-Si film (2.4×10^{-6} S/cm). It is well established that there is a large percentage of the dopant atoms did not occupy electrical active positions into the silicon, and such a behavior was obviously more pronounced in the p-type samples.[16] The conductivity of either n-a-Si or p-a-Si film is lower than that of the doped amorphous silicon film deposited by PECVD (plasma-enhanced chemical vapor deposition),[17] which could be

attributed to a large concentration of the defects, as we mentioned in the discussion of the Raman datum in Figure S2. The efficiency of the commercial a-Si solar cell with a single junction is about 8.5%,[18] which is usually prepared by the method of PECVD. In this work, the a-Si films were deposited by sputtering under our experimental conditions, which results in a large concentration of defects and a low conductivity of a-Si layers. This may be a main factor of low efficiency of PZT/a-Si cell, compared with that of the commercial a-Si solar cell.

Figure S8 shows the energy diagram of Ag/n-a-Si/PZT/ITO/glass and Ag/p-a-Si/PZT/ITO/glass samples. When an n-a-Si layer is contacted with the PZT films, the Fermi level of n-a-Si layer shifts to the conduction band so that the ΔE_e increases and the ΔE_h decreases, which is beneficial to the light-induced charges transport, as shown in Figure S8a. On the contrary, in the Ag/p-a-Si/PZT/ITO/glass sample, the ΔE_e decreases and the ΔE_h increases because the Fermi level of p-a-Si layer shifts to the valance band, as shown in Figure S8b. By the way, the ΔE_h can not be minimized to zero by adjusting the Fermi level of a-Si film due to the large band gap (3.6 eV) of PZT film. The mechanism of photovoltaic effect discussed in the Ag/a-Si/PZT/ITO/glass sample suggests that the ferroelectric PZT film is not a single candidate, and other ferroelectrics with a low band gap (2.7-3.4 eV), such as $BiFeO_3$,[19] $Bi_4Ti_3O_{12}$,[20] or $PbTiO_3$,[21] are expected to improve the photovoltaic performance of ferroelectric materials further by considering that low band gaps of these materials may be helpful for the band structure of ferroelectric/a-Si heterojunction. The coming efforts should be deserved for the photovoltaic effect of

the ferroelectrics.

Notes and references

1 D. W. Cao, C. Y. Wang, F. G. Zheng, W. Dong, L. Fang and M. R. Shen, *Nano Lett.*, 2012, **12**, 2803.

2 P. Zhang, D. W. Cao, C. Y. Wang, M. R. Shen, X. D. Su, L. Fang, W. Dong and F. G. Zheng, *Mater. Chem. and Phys.*, 2012, **135**, 304.

3 J. Kim, A. A. Kandil, K. Fogel, H. Hovel and D. K. Sadana, *ACS Nano,* 2010, **4**, 7331.

4 Z. Li, W. Li, Y. D. Jiang, H. H. Cai, Y. G. Gong and J. A. He, *J. Raman Spectrosc.*, 2011, **42**, 415.

5 K. H. Wu, X. Q. Yan and M. W. Chen, *Appl. Phys. Lett.,* 2007, **91**, 101903.

6 W. B. Wu, K. H. Wong and C. L. Choy, *Appl. Phys. Lett.,* 2004, **85**, 5013.

7 F. G. Zheng, J. Xu, L. Fang, M. R. Shen and X. L. Wu, *Appl. Phys. Lett.,* 2008, **93**, 172101.

8 D. W. Cao, J. Xu, L. Fang, W. Dong, F. G. Zheng and M. R. Shen, *Appl. Phys. Lett.,* 2010, **96**, 192101.

9 J. Xu, D. W. Cao, L. Fang, F. G. Zheng and M. R. Shen, *J. Appl. Phys.*, 2009, **106**, 113705.

10 D. W. Cao, C. Y. Wang, F. G. Zheng, L. Fang, W. Dong and M. R. Shen, *J. Mater. Chem.,* 2012, **22**, 12592.

11 J. Tauc, *Mater. Res. Bull.*, 1970, **5**, 721.

12 M. Ristova, Y. Kuo and H. H. Lee, *Appl. Sur. Sci.*, 2003, **218**, 44.

13 L. Ley and M. Cardona, *In Photoemission in Solids I*; Springer: New York, 1978.

14 G. Ertl and J. Kuppers, *Low Energy Electrons and Surface Chemistry*; VCH: Weinheim, 1985.

15 J. B. Gao, C. L. Perkins, J. M. Luther, M. C. Hanna, H. Y. Chen, O. E. Semonin, A. J. Nozik, R. J. Ellingson and M. C. Beard, *Nano Lett.*, 2011, **11**, 3263.

16 D. Girginoudi, C. Tsiarapas and N. Georgoulas, *Appl. Sur. Sci.*, 2011, **257**, 3898.

17 N. M. Liao, W. Li, Y. D. Jiang, Z. M. Wu and K. C. Qi, *Philo. Maga.*, 2008, **88**, 3051.

18 A. V. Shah, H. Schade, M. Vanecek, J. Meier, E. Vallat-Sauvain, N. Wyrsch, U. Kroll1, C. Droz1 and J. Bailat, Prog. Photovolt: Res. Appl., 2004, **12**,113.

19 X. M. Chen, H. Zhang, T. Wang, F. F. Wang and W. Z. Shi, *Phys. Status Solidi A*, 2012, **209**, 1456.

20 X. S. Wang, J. W. Zhai, L. Y. Zhang and X. Yao, *Infra. Phys. Tech.*, 1999, **40**, 55.

21 M. P. Moret, M. A. C. Devillers, K. Wörhoff and P. K. Larsen, *J. Appl. Phys.*, 2002, **92**, 468.